Connecting the Dots: A Computational Framework linking Molecular Regulation, Synaptic Plasticity, and Brain Disorders

Ze-Zheng Li[1], Wen-Hao Wu[1], Wu Li[2,3*], and Wen-Xu Wang[1,2,3,4+]

1. School of Systems Science, Beijing Normal University, Beijing, 100875, China;
2. State Key Laboratory of Cognitive Neuroscience and Learning, Beijing Normal University, Beijing 100875, China;
3. IDG/McGovern Institute for Brain Research, Beijing Normal University, Beijing 100875, China;
4. Chinese Institute for Brain Research, Beijing, 102206, China.

*Email: liwu@bnu.edu.cn

+Email: wenxuwang@bnu.edu.cn

ABSTRACT

The complexity of brain function emerges from multiscale interactions spanning molecular, synaptic, and circuit levels. While substantial progress has been made in each domain, a unified framework linking molecular perturbations to large-scale brain dysfunctions remains elusive. Here, we introduce a computational framework that bridges molecular regulation and neuronal plasticity, providing mechanistic insights into disease pathogenesis. By creating a Boolean network model of molecular regulatory pathways, we identify two stable states—synaptic potentiation and depression—governed by AMPA receptor trafficking and consistent with Hebbian learning principles. Through in silico knockout simulations mimicking genetic anomalies, our model demonstrates how molecular perturbations cascade across scales, disrupting synaptic plasticity and ultimately driving diverse neurological dysfunctions. The model's predictions align with a broad range of experimental and clinical data. Our framework establishes a mechanistic foundation for understanding the hierarchical causality of brain disorders, offering a powerful tool for dissecting disease mechanisms and informing targeted therapies.

Introduction

Synaptic plasticity is fundamental to brain functions such as perception, learning, memory, and decision-making. (*1-6*). Research on synaptic plasticity spans two major domains: neuronal electrophysiology (*7, 8*) and molecular regulation (*9, 10*). Electrophysiological studies have identified key neuronal phenomena, including synaptic potentiation and depression, particularly in regions like the hippocampus and cerebellum (*11-14*). At the molecular level, glutamatergic synaptic plasticity is mediated by the insertion and recycling of α-amino-3-hydroxy-5-methyl-4-isoxazolepropionic acid receptors (AMPARs) in the postsynaptic membrane (*9, 15*), a process modulated by N-Methyl-D-aspartic acid receptors (NMDARs) and metabotropic glutamate receptors (mGluRs) (*16, 17*). Notably, the plasticity of

engram cells in the hippocampus is thought to play a crucial role in short-term memory formation and associative learning (*18, 19*).

During brain development, synaptic pruning and proliferation are vital for neural circuit refinement and overall brain health. Dysregulation of molecular mechanisms governing synaptic plasticity has been implicated in various neurological and psychiatric disorders (*20-24*). Genetic factors, including single nucleotide polymorphisms (SNPs), gene variants, and aberrant gene expression patterns affecting neuroplasticity, are frequently observed in conditions such as Alzheimer's disease (AD), autism spectrum disorders (ASD), and schizophrenia (SCZ) (*25-28*).

Despite extensive experimental findings, a comprehensive theoretical framework and computational models are needed to fully elucidate the multiscale dynamics of synaptic plasticity. While existing models describe molecular regulation pathways (*29-32*), including receptor diffusion and trafficking, they often fail to capture the systems-level mechanisms that govern synaptic plasticity (*33*). Synaptic modifications arise from intricate biochemical interactions—including binding, assembly, catalysis, and transport—among a myriad of proteins and signaling molecules. While protein knockout studies have demonstrated correlations between synaptic plasticity and specific proteins, the broader regulatory dynamics among these molecules remain elusive (*34-37*). Reductionist approaches, which isolate molecular mechanisms, limit our understanding of how plasticity emerges from complex molecular interactions. Developing an integrative systems model that captures these interactions across multiple scales has been a critical challenge.

In this study, we construct a molecular regulatory network underlying synaptic plasticity in glutamatergic neurons, integrating existing experimental findings. In this network, nodes represent proteins and signaling molecules, while edges denote biochemical interactions. To analyze its dynamic properties, we create a biology-based Boolean network model, where each node follows a Boolean function reflecting its experimentally established biochemical role. This model identifies two stable attractors corresponding to AMPAR insertion and internalization, representing synaptic potentiation and depression, respectively. Our results show that these molecular-level dynamics are consistent with Hebbian learning principles, linking molecular regulation to neuronal plasticity (*9, 16, 20*).

Furthermore, we investigate how structural perturbations, such as protein mutations, impact network stability and dynamics. Our analysis reveals that specific mutations disrupt attractor stability, reduce the attraction basin size, and impair synaptic plasticity. By quantifying these effects, we assess the respective contributions of individual proteins to synaptic dysfunction. Comparisons with an extensive repertoire of experimental and clinical data indicate a strong correlation between mutation-induced plasticity impairments and the severity of various brain disorders. This multiscale framework bridges molecular mechanisms, synaptic plasticity, and disease pathogenesis, offering a robust basis for early diagnostics, therapeutic targets, and drug development.

Model

Synaptic plasticity regulatory network and Boolean dynamics

We constructed a regulatory network for plasticity in glutamatergic synapses, based on a comprehensive review of molecular studies (*9, 10, 15, 38-41*). This network comprises 26 nodes and 39 edges (Fig. 1), representing key proteins and signaling molecules, along with their biochemical interactions. The edges are classified into two categories of reactions: binding and catalytic regulation. Nodes connected by binding edges form protein complexes that either activate downstream proteins (activation edges) or inhibit them (inhibition edges) (see SI for details). Catalytic regulation involves activation and inhibition edges that modulate the activity of downstream nodes, either upregulating or downregulating their states.

The network includes three types of glutamate receptors—AMPAR, NMDAR, and mGluR—with AMPAR acting as the network's output and the other two as inputs (Fig. 1). The network integrates two classical pathways (*17*): the protein kinase C (PKC) pathway, activated by mGluRs; and the calmodulin pathway, triggered by calcium influx from NMDARs or calcium released from endoplasmic reticulum (ER) stores. These established pathways are further complemented by recent discoveries. For instance, Thorase facilitates synaptic depression by antagonizing the binding of N-ethylmaleimide-sensitive fusion protein (NSF) to AMPARs (*42*); and Thorase activation is aided by Nitric Oxide (*43*). All experimentally validated biochemical interactions are incorporated into the network.

To characterize the dynamics of this protein-regulatory network, we propose a biologically grounded Boolean network model, in which each node's state is either active (1) or inactive (0). A node's state (output) is determined by the states of its upstream nodes (inputs) and a corresponding Boolean function that encapsulates relevant biochemical reactions. These Boolean functions are derived from experimental findings on molecular signaling (see Supplementary Information Table S1 for details). Fig. 1 depicts the structure of the molecular regulatory network, integrating multiple signal transduction pathways. The network's state space comprises 2^{26} possible Boolean states. Exhaustively enumerating this vast state space to fully capture its dynamics would be computationally prohibitive. Instead, we adopt a biologically informed simplification to facilitate analysis.

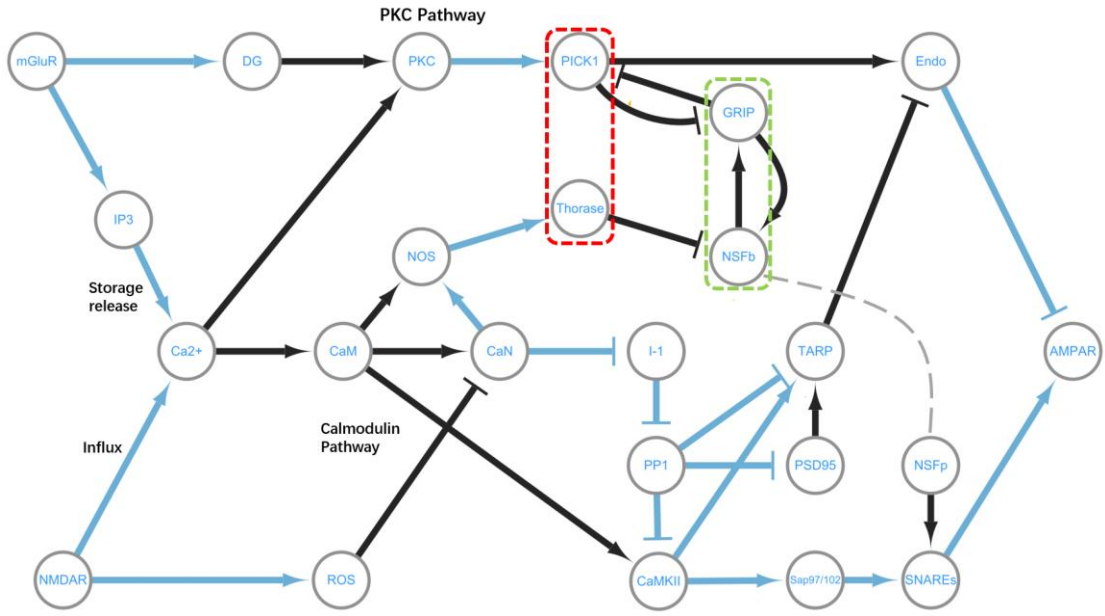

Figure 1. Full synaptic-plasticity regulation network. This network comprises 26 nodes and 39 edges, where edge color distinguishes two biochemical processes: black edges indicate binding reactions, while blue edges represent catalytic reactions. Each edge type follows two regulatory mechanisms: arrows denote activation of downstream nodes, whereas T-shaped edges denote inhibition or blocking. The network features two input nodes, mGluR and NMDAR, which activate distinct phosphorylation pathways: the PKC pathway mediated by mGluR, and the calmodulin pathway co-activated by both mGluR and NMDAR. The red and green dashed boxes highlight two pairs of auxiliary proteins that co-bind with AMPARs: PICK1 and GRIP compete for the same binding site, while Thorase and NSF bind at the same domain. NSF is depicted as two distinct nodes to reflect its dual function: NSFb represents AMPAR-bound NSF, while NSFp represents membrane-pool NSF, which assists exocytosis (dashed gray curve). These phosphorylation and dephosphorylation signals ultimately regulate endocytosis and exocytosis. For simplicity, proteins involved in exocytosis (e.g., Vamp, Syntaxin, SNAP) are consolidated into a single node, SNAREs, while the Endo node represents the protein complex responsible for endocytosis, including AP2, Dynamin, and Endophilin. Full names and Boolean functions of all nodes are provided in Supplementary Information Table S1.

Simplified Boolean network

The simplification process is guided by the principle that the reduced network must preserve the dynamics of the original. Thus, only manipulations that maintain the original network's dynamic behavior are permitted. Under this constraint, two legitimate modifications are applied: node merging and edge merging (see Fig. 8 and Table 1 in Methods). The resulting Boolean network consists of 11 nodes and 18 edges (Fig. 2), where each node may represent an aggregation of multiple original nodes. The modified Boolean functions remain consistent with experimentally validated molecular signals, as detailed in Table 3 (see Methods). This simplified network retains two input nodes: mGluR and NMDAR. In the original network, AMPAR output is jointly determined by Endo and SNAREs. Since AMPAR is fully dependent on

these two elements, it is omitted in the simplified network, leaving Endo and SNAREs as the outputs. We then use this simplified network for simulations and analyses.

The 11-node Boolean network has a theoretical state space of 2^{11} Boolean states. However, only biologically plausible input combinations are considered. For instance, the state $S_{\mathrm{mGluR}} = 0$ and $S_{\mathrm{NMDAR}} = 1$ is impossible because $S_{\mathrm{NMDAR}} = 1$ (NMDAR activation) requires glutamate release, which would also set $S_{\mathrm{mGluR}} = 1$. Applying such biological constraints eliminates 2^9 states, reducing the total number of biologically plausible Boolean states to 2^{11}-2^9=1,536.

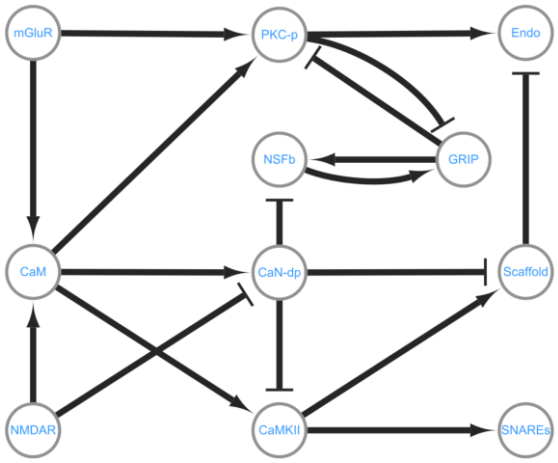

Figure 2. Simplified synaptic-plasticity regulation network. This reduced network consists of 11 nodes and 18 edges, with Boolean functions defined in Table 2. The three major pathways in the original network are streamlined as follows: CaN and PP1 are merged into a single node, CaN-dP; components of the PKC pathway are integrated into PKC-P; and auxiliary proteins for AMPAR and scaffold proteins are combined into a single Scaffold node. The criteria for these simplifications are detailed in Methods.

Results

Boolean dynamics of synaptic plasticity

We performed numerical simulations across all 1,536 biologically plausible initial Boolean states to examine their evolutionary trajectories toward final stable states. Fig. 3a shows three representative examples of evolution trajectories originating from distinct input states. After a few time steps, the system consistently settles into a stable state. Two types of attractors emerge: fixed-point attractors (Fig 3a, top and bottom panels) and period-two attractors, which oscillate between two stable states (Fig 3a, middle). Each attractor corresponds to a distinct biological function and falls into one of the three categories: synaptic potentiation ($S_{\mathrm{Endo}} = 0,\ S_{\mathrm{SNAREs}} = 1$), synaptic depression ($S_{\mathrm{Endo}} = 1,\ S_{\mathrm{SNAREs}} = 0$), and synaptic silence ($S_{\mathrm{Endo}} = 0,\ S_{\mathrm{SNAREs}} = 0$). These are denoted as P, D, and S attractor, respectively. Among them, the S attractors (bottom panel) are biologically trivial and do not contribute to

synaptic plasticity. Fig. 3b illustrates the activated nodes and edges within each attractor. In both P and D attractors, a self-sustaining regulatory structure emerges, involving NSFb and GRIP, where oscillatory activity can persist in the absence of inhibitory input to NSFb. Notably, in all attractors, at most one of the two output nodes is active at any given time.

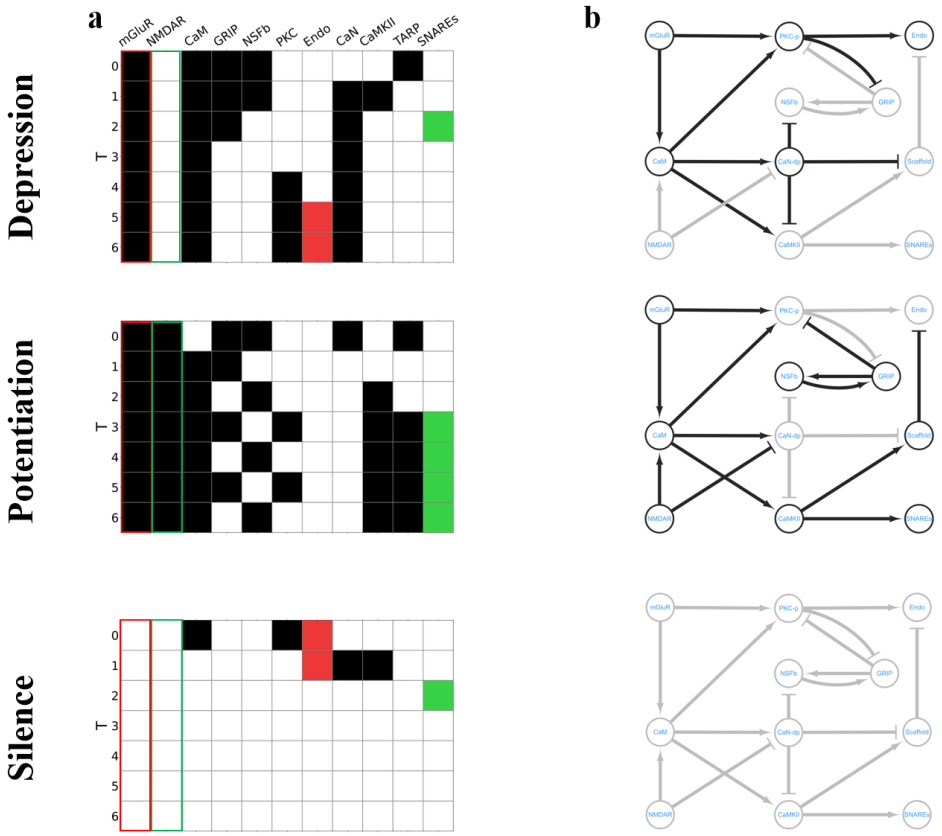

Figure 3. Evolution of node states toward attractors and active edges within each attractor. (a) Stepwise evolution of node states (T0 to T6), starting from initial states (T0), toward the depression (D), potentiation (P) and silence (S) attractors. Empty squares represent inactive state (0), while filled squares indicate active state (1). The two input nodes (mGluR and NMDAR) are outlined in red and green, respectively (two left columns), while the active states of the two output nodes (Endo and SNAREs) are highlighted with red and green squares. The P and D attractors are represented as continuous activation of SNAREs and Endo, respectively. (b) Active (black) and inactive (gray) edges when the system enters each attractor. In both D and P attractors, a self-sustaining regulatory loop involving NSFb and GRIP remains active even in the absence of upstream inhibition to NSFb.

Fig. 4 illustrates the attraction basins of P and D attractors. Each state corresponds to a point in the 11-dimensional state space, encompassing a total of 1,536 states. From any initial state, the system follows a trajectory—a sequence of states—toward a stable state. The collection of all states along these trajectories that lead to a given stable state defines its attraction basin. Both P and D attractors have distinct, non-overlapping attraction basins, meaning that any initial state leads exclusively to either synaptic potentiation or synaptic depression, but not

both. This mutual exclusivity is biologically significant, as potentiation and depression are opposing mechanisms, and their simultaneous activation would disrupt normal neuronal function. Our Boolean dynamics simulations are in line with known neuronal functions. The presence of the P attractor, associated with activation of the input node NMDAR, is consistent with the Hebbian learning rule (*44, 45*). NMDAR activation requires both glutamate release from the pre-synaptic neuron and an increase in intracellular calcium in the post-synaptic neuron—conditions that occur when pre- and post-synaptic neurons fire simultaneously. Consequently, the regulatory network settles into the P attractor, leading to synaptic potentiation, in agreement with the well-known principle: fire together, wire together.

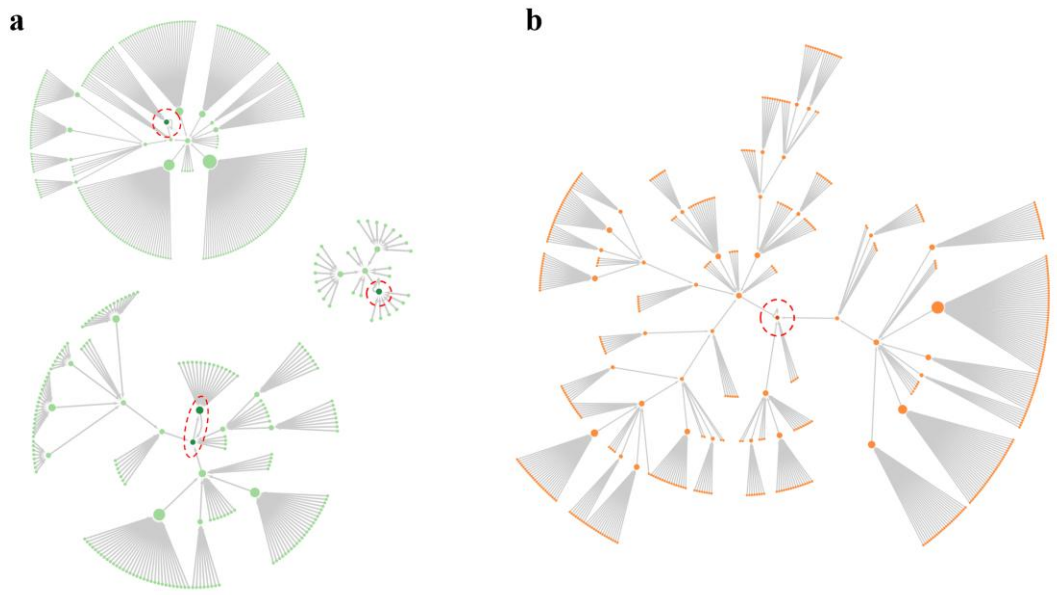

Figure 4. Attractors and their attraction basins. The P (a) and D (b) attractors, along with their respective attraction basins, are shown in green and orange. Attractors are enclosed by red dashed circles. The P attractor comprises three distinct attractors: two fixed-point attractors (a, top and right) and one limit-cycle attractor (a, bottom). In contrast, the D attractor is a single fixed-point attractor (b). The limit cycle within the P attractor stems from the self-sustaining loop in the simplified network (see Fig. 2). The size of each state node (a specific point in the state space) is proportional to the number of neighboring states connected to it.

Synaptic plasticity impairment by node knockout

To investigate how disruptions in protein interactions affect synaptic plasticity, we simulated single-node knockouts in the original full Boolean network, mimicking the effects of protein mutations. We analyzed changes in the attractors and their attraction basins in the resulting residue networks and compared them with those of the intact network.

Fig. 5 shows the residue networks resulting from single-node knockouts, together with their corresponding loss of attraction basins (a comprehensive depiction of all residue networks, including their attractors and attraction basins, is provided in Fig. S2). Note that knockouts

are applied to the original full network before undergoing the same node- and edge-merging procedures used for network simplification. As a result, different knockouts may converge into identical simplified networks. Through this process, we identified 11 distinct simplified residue networks from all single-node knockouts.

The extent of attractor and attraction basin loss serves as an indicator of synaptic plasticity impairment. However, in some cases, different knockouts result in similar degrees of basin loss, making direct comparison challenging. To refine our assessment, we introduce weighted attraction basins, which account for the relative importance of individual state nodes within each basin. Specifically, each state node is assigned a weight proportional to the number of paths passing through it toward the attractor. A state node with a larger number of paths is considered more influential since its removal disrupts multiple upstream trajectories, resulting in a greater reduction in the attraction basin. The weighted size of an attraction basin is defined as the sum of the weights of all state nodes within the basin (see Methods for details).

To quantify the degree of synaptic plasticity impairment, we define the loss of weighted attraction basin as:

$$Loss_X = \frac{B_X - B'_X}{B_X}, \mathrm{X} \in \{\mathrm{P}, \mathrm{D}\}$$

where B_X represents the weighted attraction basin size of the intact network, and B'_X denotes the corresponding size in the residue networks for both potentiation (P) and depression (D) attractors. A higher $Loss_X$ value indicates greater impairment of plasticity.

In the intact network, the attraction basins for P and D are of equal size (Fig. 5a, denoted by equally divided halves of a pie). However, following node knockouts, varying degrees of impairment emerge, which we categorize into three scenarios. (1) mild damage: both potentiation and depression functions (attractors) are preserved, despite a reduction in attraction basin size; (2) severe damage: one of the two functions is completely lost; (3) lethal damage: both functions are lost, indicating total failure of synaptic plasticity. While direct experimental validation of these predictions remains challenging, our findings can be cross-referenced with empirical evidence from clinical research on various brain disorders associated with synaptic plasticity dysfunction.

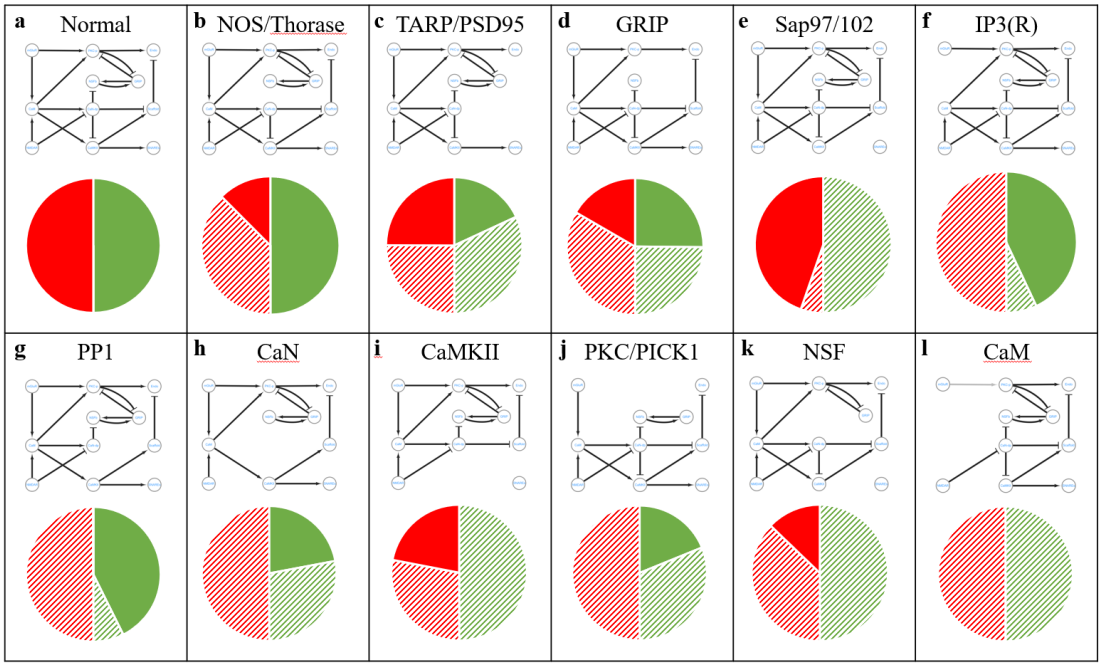

Figure 5. Residue networks and loss of attraction basins following node knockouts. (a) The intact network, with its P- and D-basin sizes represented by the green and red half-pies, respectively. (b-l) Residue networks resulting from single-node knockouts, arranged in increasing order of attraction basin loss. The shadowed sectors represent the reduction in P and D basin size relative to the intact network, illustrating the degree of synaptic plasticity impairment caused by each knockout.

Relationship between plasticity impairment and brain disorders

Extensive empirical evidence suggests that impairments in brain structures, involving both white and gray matter, contribute significantly to various brain disorders. Examples include white matter atrophy and fiber degeneration in AD, deficits in synaptic pruning in ASD, and excessive-pruning—particularly in the frontal cortex—observed in SCZ patients. The correlation between these structural abnormalities and brain disorders can be understood through the multiscale causality, which posits that both local and global neural circuits play a key role in shaping brain functions.

During critical developmental periods, the proliferation and pruning of neuronal connections are fundamental to circuit formation and the emergence of cognitive functions. Disruptions in these synaptic plasticity processes during development are implicated in the pathogenesis of many brain disorders (*46, 47*). Based on this, we hypothesize a positive correlation between the severity of brain dysfunctions and the degree of synaptic plasticity impairment. To examine this hypothesis, we leverage established genetic anomalies associated with brain diseases, as these genetic factors provide a basis for aligning our knockout simulations with specific neurological and psychiatric conditions.

Genetic studies have identified numerous disease-associated loci with mutation variations

across various brain disorders (see Table S2 for details). In our Boolean network model, node knockout operations serve as an analog to gene mutations affecting these loci. Although defining the absolute severity of brain diseases remains challenging, the World Health Organization (WHO) classifies brain diseases into two broad categories (see Table S3): diseases of the nervous system (DN) versus mental, behavioral, or neurodevelopmental disorders (MBND), with the former generally being more severe than the latter. To establish a functional link, we simulate the knockout of nodes corresponding to disease-associated gene loci in our Boolean regulatory network. After simplification and simulations, we assess changes in the P and D attraction basins of the perturbed network. In this framework, genetic anomalies serve as a bridge between the functional loss of synaptic plasticity—quantified by our model—and the severity of brain diseases based on clinical evidence. Consequently, this approach provides a causal framework to test our hypothesis regarding the close relationship between synaptic plasticity dysfunction and brain disease severity.

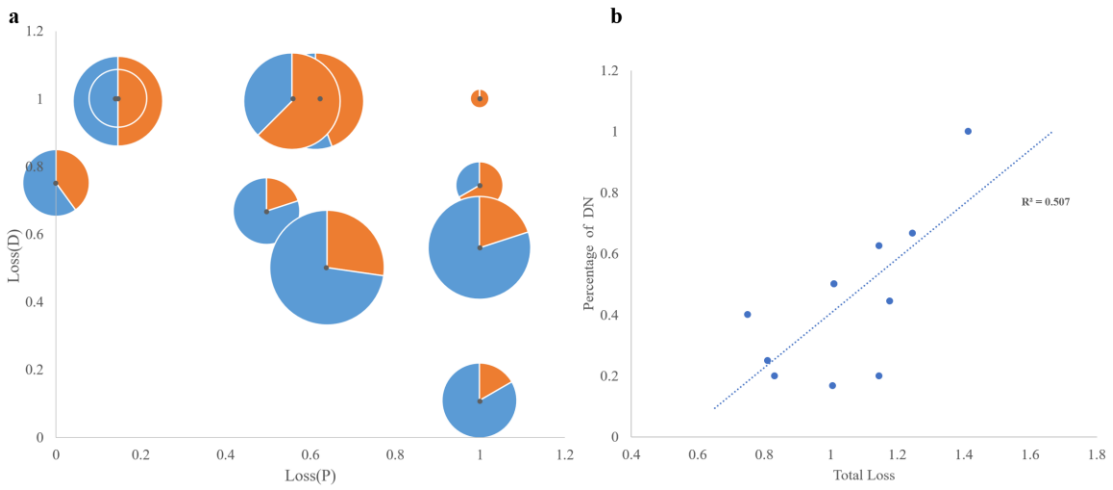

Figure 6. Relationship between the loss of attraction basins and the severity of brain diseases. (a) Loss of P- and D-attraction basins (x- and y-axis, respectively) following the knockout of individual nodes in the original network. Each pie chart represents a different knockout, with the pie center indicating the reduction in attraction basin size. Pie size is proportional to the number of brain disease types associated with the corresponding gene deficit; orange and blue sectors denote DN and MBND cases, respectively. (b) Severity of brain diseases as a function of the total loss of attraction basins. Each data point corresponds to a pie chart in (a). The severity of each knockout is quantified as the percentage of the orange (DN) sector within the corresponding pie; the total loss is defined as the distance of the pie center from the origin. Detailed disease information is presented in Table S2.

Fig. 6a shows the relationship between P- and D-basin loss and the severity of brain disorders. Each pie represents the knockout of a protein or the mutation of the corresponding gene. The coordinates of each pie's center denote the extent of P- and D-basin loss, while the proportion of orange and blue colors indicates the prevalence of DN and MBND cases, respectively. Generally, when P- and D-basin loss is relatively small (closer to the bottom-left corner), DN

cases are fewer, as reflected by the smaller orange sectors. Conversely, when both P- and D-basin loss is relatively large (closer to the upper-right corner), DN cases predominate, with orange sectors comprising more than half of the pie. Fig. 6b reveals a significantly positive correlation between total attraction-basin loss and brain disease severity ($P<0.01$, t-test), providing strong support for the multiscale causality and validating our Boolean network approach.

Among all brain disorders, neuroimaging studies and postmortem analyses of ASD and SCZ patients have explicitly demonstrated abnormalities in neuronal connectivity. Adolescent ASD patients often exhibit a thicker cortex than healthy individuals, particularly in the frontal, temporal and parietal lobes (*48, 49*). In contrast, SCZ is characterizes by synaptic atrophy and reduced cortical thickness, especially in the frontal and temporal lobes, primary auditory cortex, and hippocampus (*49, 50*). These morphological anomalies suggest that ASD and SCZ may result from synaptic plasticity dysfunctions. To investigate this, we utilize node knockout analysis in our Boolean regulatory network to gain deeper insights into the neuronal mechanisms driving these disorders.

Focusing on gene loci typically associated with ASD and SCZ, we align plasticity impairments in our network with neuroanatomical abnormalities observed in these conditions. Fig. 7 quantifies P- and D-basin loss (green and red bars, respectively) resulting from specific gene mutations linked to ASD and SCZ. Our results demonstrate differential impacts on plasticity functions in the two disorders: In ASD, synaptic depression impairment is more pronounced than potentiation impairment, whereas the opposite trend is observed in SCZ. These findings offer a molecular-level explanation for the distinct cortical abnormalities seen in ASD and SCZ: In ASD, the impaired depression function results in insufficient synaptic pruning during brain development, promoting excessive synaptic retention and cortical thickening; by contrast, in SCZ, the impaired potentiation function hinders synaptic strengthening and connectivity, causing excessive pruning and cortical thinning.

Among the mutated genes, GRIP is notable for being implicated in both ASD and SCZ. Its knockout leads to relatively mild impairments in both potentiation and depression functions. To quantify this residual plasticity, we introduce a metric assessing the remaining functional capacity of the network. The analysis suggests that GRIP mutations preserve more plasticity than mutations in other disease-associated genes. We speculate that GRIP dysfunction, as a shared comorbid factor in ASD and SCZ, may establish a compensatory balance between potentiation and depression, resulting in comparatively milder symptoms.

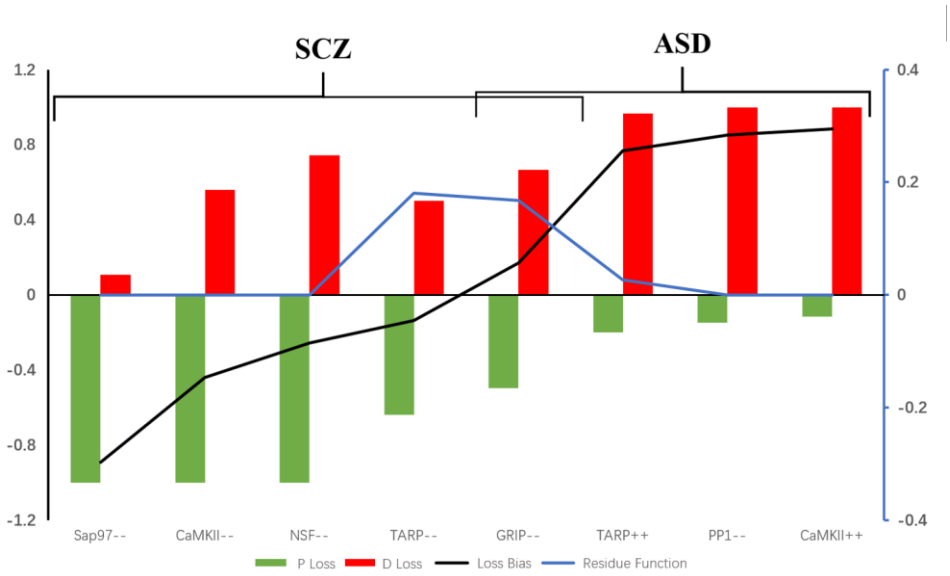

Figure 7. Modeling gene mutations in SCZ and ASD using Boolean network simulations. Clinical studies have identified 5 deficit-associated gene loci in SCZ and 4 in ASD, with GRIP implicated in both disorders. These loci are ordered by ascending difference between knockout-induced D-basin loss (red) and P-basin loss (green). Black curve represents the imbalance between P- and D-basin loss, calculated as their difference. Blue curve denotes the residue function, capturing node-specific anomalies, computed as $\frac{B'_D \cdot B'_P}{B_D \cdot B_P}$. Node annotations: (--) low expression or locational variation; (++) overexpression. Simulations of TARP and CaMKII overexpression are detailed in the Supplementary Information and Fig. S2.

Discussion

Plasticity is a fundamental property of the brain, enabling adaptation through dynamic modifications in neuronal structure and function. Despite extensive research on neuroplasticity and a wealth of molecular and synaptic findings, the absence of a unified theoretical and computational framework at the systems level continues to hinder a deeper understanding of how neuronal networks self-organize and operate in both health and disease. This study addresses this gap by establishing causal links between molecular regulation, synaptic plasticity, and brain disorders.

Focusing on glutamatergic neurons—the predominant neuronal type in the brain—we constructed a molecular regulatory network of synaptic plasticity. This network comprises proteins and signaling molecules that mediate a vast array of biochemical interactions. To manage this biological complexity while preserving essential functions, we developed a Boolean network model, which captures key regulatory interactions while maintaining computational tractability. Each node was assigned a Boolean function derived from experimental data and established molecular mechanisms. Since the full network remains computationally prohibitive due to its high-dimensional state space (26 dimensions and 2^{26} possible states), we introduced two simplifications that preserve its dynamic properties. The resulting Boolean network exhibits two types of attractors and their associated attraction

basins, corresponding to the insertion and internalization of AMPARs. These AMPAR-related processes, jointly regulated by NMDARs and mGluRs, govern synaptic potentiation and depression, effectively recapitulating the fundamental mechanisms of synaptic plasticity. Moreover, the Boolean network adheres to Hebbian learning principles, as NMDAR activation—indicating concurrent pre- and post-synaptic activity—drives the system toward the potentiation attractor, aligning with the classic rule: “fire together, wire together”.

Using this Boolean network, we conducted node-knockout studies to simulate gene mutations linked to neurodevelopmental disorders. These perturbations enabled us to examine the relationship between attractor loss and disease severity, allowing validation of our model against empirical and clinical findings. Strikingly, we found that the extent of attractor loss positively correlates with disease severity, as documented by WHO criteria. Among various neuropsychiatric conditions, we focused on ASD and SCZ due to their well-documented structural abnormalities. Specifically, ASD and SCZ exhibit opposing trends in white matter development—insufficient pruning in ASD and excessive pruning in SCZ. When aligned with the genetic mutations associated with these disorders, our model predicts corresponding impairments in synaptic depression and potentiation, mirroring the pruning deficits observed in ASD and SCZ. These knockout studies, in agreement with clinical data, validate our Boolean network and its dynamic properties. More importantly, our model provides a framework for investigating the causal relationships between genetic anomalies, plasticity deficits, and neurofunctional disorders, offering insights that may aid in identifying molecular targets for therapeutic intervention (*51*).

Our study advances the systems-level understanding of neuroplasticity but does not yet incorporate receptor subtypes, receptor expression dynamics, or nuclear transport mechanisms (*20, 52, 53*). Beyond postsynaptic plasticity, presynaptic neurotransmitter release is regulated by signals such as nitric oxide (NO) (*17, 54, 55*) and endogenous cannabinoids (*56, 57*), which play critical roles in presynaptic adaptation—an essential process for normal neuroplasticity. In addition, neurons that utilize other neurotransmitters, including dopamine (*58, 59*), acetylcholine (*60*), and γ-aminobutyric acid (GABA) (*61*), also exhibit plasticity, albeit through distinct mechanisms. Moreover, glial cells actively contribute to neuronal growth, myelination, metabolic homeostasis, and synaptic plasticity (*20, 62, 63*). During neural development, neural precursor differentiation and growth factor-guided migration further enrich the complexity of plasticity regulation, warranting further investigation.

Although the pathophysiology of some brain disorders, such as Huntington's disease, is well-documented, the molecular mechanisms underlying most neurological conditions remain poorly understood. In many cases, only genetic associations have been identified, while their causal mechanisms remain elusive. Furthermore, the heterogeneity of brain disorders—arising from polygenic influences and comorbid conditions—complicates efforts to establish causal links between genetic mutations and clinical symptoms. While our computational framework provides a new approach to addressing these complexities, neuroscience is still in its early stages, lacking universal principles or a cohesive theoretical foundation. Given the

brain's complexity, one might ask whether neuroscience could ever develop a unifying paradigm akin to those in physics. This question extends beyond neuroscience, resonating across all complex systems research.

Emergence is a common feature of complex systems, from bacterial colonies to human societies. The aphorism "the whole is greater than the sum of its parts" encapsulates this idea. In the broader fields of biological and medical sciences, the disconnect between rapid experimental progress and slower advances in theoretical modeling calls for a paradigm shift. While experiments generate vast amounts of correlative data, establishing causal relationships across multiple scales remains a formidable challenge. Understanding complex biological systems is akin to solving a jigsaw puzzle: without knowing how individual pieces interconnect, assembling the complete picture is impossible. At present, experimental findings provide fragmented insights at either the molecular or functional level, underscoring the need for fundamental principles and systems-level models that integrate these disparate observations into a coherent framework.

Traditional differential equation-based models often become intractable when applied to high-dimensional systems like large-scale molecular regulatory networks. Thus, coarse-grained modeling approaches are indispensable for achieving an optimal balance between model accuracy and computational feasibility. Boolean dynamics, with their discrete state space, provide an efficient alternative to differential equations. As demonstrated in this study, despite simplifying certain molecular details, Boolean models remain effective in characterizing reaction processes and their biological consequences, highlighting their analytical power. However, constructing a reliable Boolean regulatory network requires comprehensive knowledge of the underlying biochemistry to ensure biologically meaningful functional representation.

Inspired by recent breakthroughs in deep learning for protein structure prediction, one may wonder whether artificial intelligence could be leveraged to decipher molecular dynamics. However, due to the emergent properties of complex systems, the organizational complexity of protein-protein interaction networks far exceeds that of individual protein folding. The lack of training data on self-organizing principles and network dynamics remains a major limitation. As a result, current data-driven approaches in artificial intelligence are insufficient for modeling molecular and circuit-level dynamics, leaving scientific intuition and mechanistic understanding indispensable (*64, 65*).

Methods

Network Simplification

The core principle of network simplification is to preserve the dynamics of the original network, ensuring that its evolutionary trajectory and steady states remain unchanged. To achieve this, only two simplification operations are permitted: edge merging and node merging. Specifically, if multiple edges of the same type (either activation or inhibition) exist between two nodes,

they are combined into a single edge (Fig. 8a, top vs. middle row). If three nodes form a unidirectional activation chain, the middle node is merged with its downstream node (Fig. 8a, middle vs. bottom row). Similarly, if three nodes form an inhibition chain, the middle node is merged with the last node, and the inhibition chain is converted into a single activation edge (Fig. 8b). These operations preserve the input-output relationships across all original pathways, ensuring that the simplified network maintains the same attractors as the original. A comprehensive list of possible simplifications is provided in Table 1.

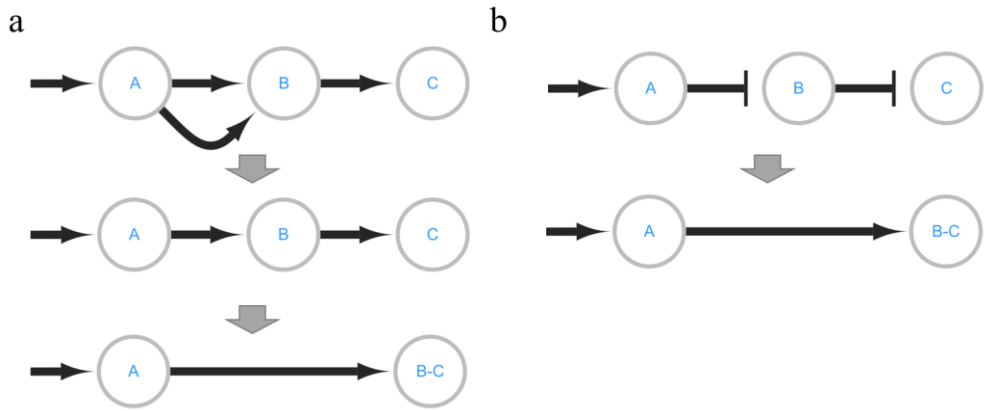

Figure 8. Schematic of network simplification operations. (a) In activation chains, edge and node merging results in a single activation edge. (b) In inhibition chains, node merging converts two consecutive inhibition edges into a single activation edge.

Table 1. Pathway shortening in the original Boolean network.

Original Nodes and Edges	**Nodes and Edges after Simplification**
mGluR → DG → PKC → PICK1	mGluR → PKC-p*
mGluR→IP3R→Ca2+→CaM	mGluR → CaM
→ Ca2+ → CaM →	→ CaM →
CaN—I I-1 —I PP1—I CaMKII	CaN-dp* —I CaMKII
CaN-dp* → NOS→ Thorase —I NSFb	CaN-dp* —I NSFb
NMDAR → ROS —I CaN	NMDAR —I CaN-dp*
CaMKII → Sap97 → SNAREs	CaMKII → SNAREs
PSD95 → TARP —I Endo	Scaffold* —I Endo

Note： Nodes marked with '*' derive from node merging.

After simplification, the network consists of 12 nodes, including the output node AMPAR. However, because AMPAR's state is fully determined by two antagonistic nodes, Endo and SNAREs, we omit it, yielding an 11-node network (Fig. 2). The Boolean functions assigned to these nodes are provided in Table 2.

Table 2. Boolean functions of nodes in the simplified Boolean network.

Nodes Name	Boolean Function	States Detail			
PKC-p	$S_{PKC_p}(t+1) =$ $S_{mGluR}(t)$ AND $S_{CaM}(t)$ AND NOT $S_{GRIP}(t)$	$S_{mGluR}(t)$	$S_{CaM}(t)$	$S_{GRIP}(t)$	$S_{PKC_p}(t+1)$
		0	0	0	0
		0	1	0	0
		1	0	0	0
		1	1	0	1
		0	0	1	0
		0	1	1	0
		1	0	1	0
		1	1	1	0
CaM	$S_{CaM}(t+1) =$ $S_{mGluR}(t)$ OR $S_{NMDAR}(t)$	$S_{mGluR}(t)$	$S_{NMDAR}(t)$	$S_{CaM}(t+1)$	
		0	0	0	
		0	1	1	
		1	0	1	
		1	1	1	
CaN-dP	$S_{CaN-dp}(t+1) =$ $S_{CaM}(t)$ AND NOT $S_{NMDAR}(t)$	$S_{CaM}(t)$	$S_{NMDAR}(t)$	$S_{CaN-dp}(t+1)$	
		0	0	0	
		0	1	0	
		1	0	1	
		1	1	0	
NSFb	$S_{NSFb}(t+1) =$ $S_{GRIP}(t)$ AND NOT $S_{CaN-dp}(t)$	$S_{GRIP}(t)$	$S_{CaN-dp}(t)$	$S_{NSFb}(t+1)$	
		0	0	0	
		0	1	0	
		1	0	1	
		1	1	0	
GRIP	$S_{GRIP}(t+1) =$ $S_{NSFb}(t)$ AND NOT $S_{PKC-p}(t)$	$S_{NSFb}(t)$	$S_{PKC-p}(t)$	$S_{GRIP}(t+1)$	
		0	0	0	
		0	1	0	
		1	0	1	
		1	1	0	
CaMKII	$S_{CaMKII}(t+1) =$ NOT $S_{CaN-dp}(t)$ AND $S_{CaM}(t)$	$S_{CaM}(t)$	$S_{CaN-dp}(t)$	$S_{CaMKII}(t+1)$	
		0	0	0	
		0	1	0	
		1	0	1	
		1	1	0	
Scaffold	$S_{Scaffold}(t+1) =$ NOT $S_{CaN-dp}(t)$ OR $S_{CaMKII}(t)$	$S_{CaN-dp}(t)$	$S_{CaMKII}(t)$	$S_{Scaffold}(t+1)$	
		0	0	0	
		0	1	1	
		1	0	0	
		1	1	0	
Endo	$S_{Endo}(t+1) =$	$S_{PKC-p}(t)$	$S_{Scaffold}(t)$	$S_{Endo}(t+1)$	

	$S_{PKC-p}(t)$ AND NOT $S_{Scaffold}(t)$	0	0	0
		0	1	0
		1	0	1
		1	1	0
SNAREs	$S_{SNAREs}(t+1) = S_{CaMKII}(t)$	$S_{CaMKII}(t)$		$S_{SNAREs}(t+1)$
		0		0
		1		1

Boolean Dynamics

For any arbitrary node i, its state $s_i(t)$ at time t is determined by its Boolean function and its upstream inputs. The network's global state $S(t)$ is defined as the collective states of all nodes:

$$S(t) = \{s_1(t), s_2(t), s_3(t), \cdots, s_n(t)\}$$

This collection of all possible states forms the network's state space. In a convergent system, any initial state ultimately evolves into a steady configuration, known as an attractor. There are two types of attractors: fixed points, where the network settles into a single steady state; and limit cycles, where the system oscillates between multiple states. Once an attractor is reached, the system's global state S repeats a previously visited configuration. By enumerating all initial states, we derive the complete set of evolutionary trajectories and their corresponding attractors. The number of states that eventually lead to an attractor defines the size of its basin of attraction. In deterministic Boolean networks, each state S belongs to exactly one attractor, ensuring that attraction basins do not overlap.

Weighted Attraction-basin Size

As shown in Fig. 4, within the Boolean network's state space, each attractor's basin of attraction forms a tree-like structure, where multiple branches originating from different initial states gradually converge toward the attractor. In this hierarchical structure, state nodes occupy different levels, reflecting their varying influences on network dynamics. Roughly speaking, state nodes with a greater number of incoming paths play a more central role in determining the network's final behavior. To quantify this influence, we assign a weight to each state node based on the number of paths passing through it. The weighted attraction-basin size is then defined as the sum of the weights of all state nodes:

$$B_{P/D} = \sum_{i \in P/D} b(i),$$

Where $b(i)$ denotes the number of paths passing through state node i, P/D represents all states that evolve toward either the P or D attractor, and $B_{P/D}$ corresponds to the weighted size of the respective attraction basin.

Reference

1. J. Sharma, A. Angelucci, M. Sur, Induction of visual orientation modules in auditory cortex. *Nature* **404**, 841-847 (2000).

2. P. Caroni, F. Donato, D. Muller, Structural plasticity upon learning: regulation and functions. *Nature Reviews Neuroscience* **13**, 478-490 (2012).
3. G. Neves, S. F. Cooke, T. V. P. Bliss, Synaptic plasticity, memory and the hippocampus: a neural network approach to causality. *Nature Reviews Neuroscience* **9**, 65-75 (2008).
4. S. J. Martin, P. D. Grimwood, R. G. M. Morris, Synaptic Plasticity and Memory: An Evaluation of the Hypothesis. *Annual Review of Neuroscience* **23**, 649-711 (2000).
5. A. Citri, R. C. Malenka, Synaptic Plasticity: Multiple Forms, Functions, and Mechanisms. *Neuropsychopharmacology* **33**, 18-41 (2008).
6. W. Li, Perceptual Learning: Use-Dependent Cortical Plasticity. *ANNUAL REVIEW OF VISION SCIENCE* **2**, 109-130 (2016).
7. R. A. Nicoll, A Brief History of Long-Term Potentiation. *Neuron* **93**, 281-290 (2017).
8. Y. Dan, M.-M. Poo, Spike Timing-Dependent Plasticity: From Synapse to Perception. *Physiological Reviews* **86**, 1033-1048 (2006).
9. G. L. Collingridge, J. T. Isaac, Y. T. Wang, Receptor trafficking and synaptic plasticity. *Nature Reviews Neuroscience* **5**, 952-962 (2004).
10. J. G. Hanley, The Regulation of AMPA Receptor Endocytosis by Dynamic Protein-Protein Interactions. *Front Cell Neurosci* **12**, 362 (2018).
11. G.-q. Bi, M.-m. Poo, Synaptic Modifications in Cultured Hippocampal Neurons: Dependence on Spike Timing, Synaptic Strength, and Postsynaptic Cell Type. *Journal of Neuroscience* **18**, 10464-10472 (1998).
12. T. V. P. Bliss, T. Lømo, Long-lasting potentiation of synaptic transmission in the dentate area of the anaesthetized rabbit following stimulation of the perforant path. *The Journal of Physiology* **232**, 331-356 (1973).
13. S. M. Dudek, M. F. Bear, Homosynaptic long-term depression in area CA1 of hippocampus and effects of N-methyl-D-aspartate receptor blockade. *Proceedings of the National Academy of Sciences of the United States of America* **89**, 4363-4367 (1992).
14. J. T. R. Isaac, R. A. Nicoll, R. C. Malenka, Evidence for silent synapses: Implications for the expression of LTP. *Neuron* **15**, 427-434 (1995).
15. M. Sheng, M. J. Kim, Postsynaptic signaling and plasticity mechanisms. *Science (New York, N.Y.)* **298**, 776-780 (2002).
16. C. Hammond, *Cellular and Molecular Neurophysiology*. (Academic Press, ed. 5, 2024), pp. 350.
17. A. Reiner, J. Levitz, Glutamatergic Signaling in the Central Nervous System: Ionotropic and Metabotropic Receptors in Concert. *Neuron* **98**, 1080-1098 (2018).
18. A. Guskjolen, M. S. Cembrowski, Engram neurons: Encoding, consolidation, retrieval, and forgetting of memory. *Molecular Psychiatry* **28**, 3207-3219 (2023).
19. S. A. Josselyn, S. Köhler, P. W. Frankland, Finding the engram. *Nature Reviews Neuroscience* **16**, 521-534 (2015).
20. L. Q. Luo, *Principles of Neurobiology(2nd ed.)*. (Garland Science, 2020).
21. M. P. Mattson, K. Moehl, N. Ghena, M. Schmaedick, A. Cheng, Intermittent metabolic switching, neuroplasticity and brain health. *Nature Reviews Neuroscience* **19**, 81-94 (2018).
22. R. B. Price, R. Duman, Neuroplasticity in cognitive and psychological mechanisms of depression: an integrative model. *Molecular Psychiatry* **25**, 530-543 (2020).

23. J. T. Ting, J. Peca, G. Feng, Functional Consequences of Mutations in Postsynaptic Scaffolding Proteins and Relevance to Psychiatric Disorders. *Annual Review of Neuroscience* **35**, 49-71 (2012).
24. A. N. Tartt, M. B. Mariani, R. Hen, J. J. Mann, M. Boldrini, Dysregulation of adult hippocampal neuroplasticity in major depression: pathogenesis and therapeutic implications. *Molecular Psychiatry* **27**, 2689-2699 (2022).
25. J. Soler *et al.*, Genetic variability in scaffolding proteins and risk for schizophrenia and autism-spectrum disorders: a systematic review. *Journal of Psychiatry & Neuroscience* **43**, 223-244 (2018).
26. D. H. Ebert, M. E. Greenberg, Activity-dependent neuronal signalling and autism spectrum disorder. *Nature* **493**, 327-337 (2013).
27. S. Kocahan, Z. Dogan, Mechanisms of Alzheimer's Disease Pathogenesis and Prevention: The Brain, Neural Pathology, N-methyl-D-aspartate Receptors, Tau Protein and Other Risk Factors. *Clinical Psychopharmacology and Neuroscience* **15**, 1-8 (2017).
28. A. Ghosh, K. P. Giese, Calcium/calmodulin-dependent kinase II and Alzheimer's disease. *Molecular Brain* **8**, (2015).
29. G. Antunes, F. M. Simoes-de-Souza, AMPA receptor trafficking and its role in heterosynaptic plasticity. *Scientific Reports* **8**, 10349 (2018).
30. P. E. Barbano *et al.*, A mathematical tool for exploring the dynamics of biological networks. *Proceedings of the National Academy of Sciences* **104**, 19169-19174 (2007).
31. A. R. Gallimore, A. R. Aricescu, M. Yuzaki, R. Calinescu, A Computational Model for the AMPA Receptor Phosphorylation Master Switch Regulating Cerebellar Long-Term Depression. *PLOS Computational Biology* **12**, e1004664 (2016).
32. M. K. Bell, P. Rangamani, Crosstalk between biochemical signalling network architecture and trafficking governs AMPAR dynamics in synaptic plasticity. *The Journal of Physiology* **601**, 3377-3402 (2023).
33. C. T. Lee, M. Bell, M. Bonilla-Quintana, P. Rangamani, Biophysical Modeling of Synaptic Plasticity. **53**, 397-426 (2024).
34. G. L. Caldeira *et al.*, Aberrant hippocampal transmission and behavior in mice with a stargazin mutation linked to intellectual disability. *Molecular Psychiatry* **27**, 2457-2469 (2022).
35. A. S. Kato *et al.*, Forebrain-selective AMPA-receptor antagonism guided by TARP gamma-8 as an antiepileptic mechanism. *Nature Medicine* **22**, 1496-+ (2016).
36. Y. P. Yang *et al.*, Reversible blockade of experience-dependent plasticity by calcineurin in mouse visual cortex. *Nature Neuroscience* **8**, 791-796 (2005).
37. M. P. Maher, J. A. Matta, S. Gu, M. Seierstad, D. S. Bredt, Getting a Handle on Neuropharmacology by Targeting Receptor-Associated Proteins. *Neuron* **96**, 989-1001 (2017).
38. I. Song, R. L. Huganir, Regulation of AMPA receptors during synaptic plasticity. *Trends in neurosciences* **25**, 578-588 (2002).
39. J. Lisman, H. Schulman, H. Cline, The molecular basis of CaMKII function in synaptic and behavioural memory. *Nature Reviews Neuroscience* **3**, 175-190 (2002).
40. J. D. Shepherd, R. L. Huganir, The cell biology of synaptic plasticity: AMPA receptor trafficking. *Annual review of cell and developmental biology* **23**, 613-643 (2007).

41. Richard L. Huganir, Roger A. Nicoll, AMPARs and Synaptic Plasticity: The Last 25 Years. *Neuron* **80**, 704-717 (2013).
42. J. Zhang *et al.*, The AAA⁺ ATPase Thorase Regulates AMPA Receptor-Dependent Synaptic Plasticity and Behavior. *Cell* **145**, 284-299 (2011).
43. G. K. E. Umanah *et al.*, AMPA Receptor Surface Expression Is Regulated by S-Nitrosylation of Thorase and Transnitrosylation of NSF. *Cell Reports* **33**, (2020).
44. R. G. Morris, *D.O. Hebb: The Organization of Behavior, Wiley: New York; 1949*. Brain Res Bull (ed. 2000/01/22, 1999), vol. 50, pp. 437.
45. J. Lisman, A Mechanism for The Hebb And the Anti-Hebb Processes Underlying Learning and Memory. *Proceedings of the National Academy of Sciences of the United States of America* **86**, 9574-9578 (1989).
46. R. M. Meredith, in *Environmental Experience and Plasticity of the Developing Brain*. (2016), pp. 73-98.
47. M. P. Forrest, E. Parnell, P. Penzes, Dendritic structural plasticity and neuropsychiatric disease. *Nature Reviews Neuroscience* **19**, 215-234 (2018).
48. P. Penzes, M. E. Cahill, K. A. Jones, J.-E. VanLeeuwen, K. M. Woolfrey, Dendritic spine pathology in neuropsychiatric disorders. *Nature Neuroscience* **14**, 285-293 (2011).
49. L. A. Glantz, D. A. Lewis, Dendritic Spine Density in Schizophrenia and Depression. *Archives of General Psychiatry* **58**, 203-203 (2001).
50. D. A. Lewis, P. Levitt, Schizophrenia as a Disorder of Neurodevelopment. *Annual Review of Neuroscience* **25**, 409-432 (2002).
51. A. S. Kato, J. M. Witkin, Protein complexes as psychiatric and neurological drug targets. *Biochemical Pharmacology* **151**, 263-281 (2018).
52. M. J. Kennedy, M. D. Ehlers, Organelles and Trafficking Machinery for Postsynaptic Plasticity. *Annual Review of Neuroscience* **29**, 325-362 (2006).
53. J. W. Hell, How Ca2+-permeable AMPA receptors, the kinase PKA, and the phosphatase PP2B are intertwined in synaptic LTP and LTD. *Science Signaling* **9**, pe2-pe2 (2016).
54. P. Picón-Pagès, J. Garcia-Buendia, F. J. Muñoz, Functions and dysfunctions of nitric oxide in brain. *Biochimica et Biophysica Acta (BBA) - Molecular Basis of Disease* **1865**, 1949-1967 (2019).
55. U. Förstermann, W. C. Sessa, Nitric oxide synthases: regulation and function. *European Heart Journal* **33**, 829-837 (2011).
56. R. I. Wilson, R. A. Nicoll, Endogenous cannabinoids mediate retrograde signalling at hippocampal synapses. *Nature* **410**, 588-592 (2001).
57. B. D. Heifets, P. E. Castillo, Endocannabinoid Signaling and Long-Term Synaptic Plasticity. *Annual Review of Physiology* **71**, 283-306 (2009).
58. P. Calabresi, B. Picconi, A. Tozzi, M. Di Filippo, Dopamine-mediated regulation of corticostriatal synaptic plasticity. *Trends in neurosciences* **30**, 211-219 (2007).
59. M. Pignatelli, A. Bonci, Role of Dopamine Neurons in Reward and Aversion: A Synaptic Plasticity Perspective. *Neuron* **86**, 1145-1157 (2015).
60. C. Kraus, E. Castren, S. Kasper, R. Lanzenberger, Serotonin and neuroplasticity - Links between molecular, functional and structural pathophysiology in depression. *Neuroscience and Biobehavioral Reviews* **77**, 317-326 (2017).
61. K. A. Pelkey *et al.*, Hippocampal GABAergic Inhibitory Interneurons. *Physiological Reviews*

97, 1619-1747 (2017).

62. P. G. Haydon, Glia: listening and talking to the synapse. *Nature Reviews Neuroscience* **2**, 185-193 (2001).
63. C. Eroglu, B. A. Barres, Regulation of synaptic connectivity by glia. *Nature* **468**, 223-231 (2010).
64. M. Mitchell, Debates on the nature of artificial general intelligence. *Science (New York, N.Y.)* **383**, eado7069.
65. M. Mitchell, *Artificial Intelligence: A Guide for Thinking Humans*. (Farrar, Straus and Giroux, ed. First Edition, 2019).